Direct Measurement of Single Synthetic Vertebrate Thick Filament Elasticity Using Nanofabricated Cantilevers

Dwayne Dunaway, Mark Fauver, and Gerald Pollack
Department of Bioengineering, University of Washington, Seattle, Washington 98195, USA

ABSTRACT Thick filaments are generally thought to be effectively inextensible. Here we use novel nanofabricated cantilevers to carry out the first direct force-elongation measurements on single vertebrate thick filaments. Cantilevers are ideal for these experiments: force ranges are from pico- to micronewtons, specimens can be visualized during the experiment, and attachment surfaces are in the same plane as the filament. Synthetic thick filaments from rabbit myosin were suspended between two cantilevers and stretched. With stretch, stiffness increased gradually and then became nearly constant after ~100 pN. Stretch rate had little or no effect on force-elongation behavior. Under physiological loads (~240 pN axially averaged with full activation) filaments elongated by 1.1 ± 0.3%. Previous x-ray diffraction results showed a 1.0 to 1.5% increase in myosin head spacing with activation; however, this increase in spacing has been interpreted as change in the state of the cross-bridges, not as elasticity in the thick filament backbone. Comparison with our data suggests that changes in the myosin x-ray reflections seen during activation may be due to elongation of the thick filament backbone. Recognition of thick filament elasticity is important because it affects the interpretation of mechanical experiments and inferences drawn on the molecular mechanism of contraction.

INTRODUCTION

With the advent of single filament techniques it has become possible to study the mechanical behavior of muscle filaments in isolation. So far, mechanical studies conducted on titin (Kellermayer et al., 1997; Rief et al., 1997; Tskhovrebova et al., 1997) and actin filaments (Kojima et al., 1994) have provided new insights into how muscle dynamics are impacted at the level of the individual filament. Elongation in the thin filament, thought to be only 0.2% to 0.3% with full isometric activation (Kojima et al., 1994; Huxley et al., 1994), has been the focus of many studies (Huxley et al., 1994; Kojima et al., 1994; Higuchi et al., 1995; Daniel et al., 1998). Even these low levels of compliance have significantly impacted the interpretation of force response to quick length changes (Ford et al., 1977), actin-myosin binding-site alignment, the stoichiometry of cross-bridge binding, and the theorized cycling rate (Daniel et al., 1998). Here we report that relative thick filament elongation is five times greater than that observed for thin filaments, a result with important consequences for the field of muscle mechanics.

MATERIALS AND METHODS

Myosin purification and filamentogenesis

Myosin was purified from rabbit psoas muscle (Margossian and Lowey, 1982; Gordon et al., 1997) and kindly donated by Ying Chen and Bryant Chase. This myosin is routinely used in in vitro motility assay experiments. The filaments are formed by gradual dilution from high to low salt concentrations with millimolar amounts of inorganic phosphate and $MgCl_2$ (Pinset-Harstrom and Truffy, 1979). The high and low salt dilution solution compositions were 500 mM KCl or 80 mM KCl, 5 mM $MgCl_2$, 0.5 mM K_2PO_4, and 10 mM Imidizole with a pH 6.8 at room temperature. Myosin (33 mg in 200 μL of 50% glycerol and 50% buffer, the latter consisting of 0.6 M KCl and 0.05 M potassium phosphate, pH 6.5) was placed in 4 mL of high KCl solution. This solution was gradually diluted with 46 mL of low KCl solution while stirring gently. Gradual dilution was accomplished with a peristaltic pump (Cole Palmer model #7519-10, Bernonhills, IL) over a period of ~2 h (0.4 mL/min). Our experience is that the rate is not critical but should be held constant to ensure proper filament formation. The longest filaments were formed with initial myosin concentrations of 0.7 mg/mL. Before mechanical experiments, filaments were diluted approximately 100 to 200 times in the following relaxation buffer: 100 mM KCl, 1 mM $MgCl_2$, 5 mM EGTA, 5 mM ATP, and 5 mM Tris with a pH of 7 at room temperature (Kubota et al., 1983; Neumann et al., 1998).

Filament imaging

The filaments were imaged in DIC (differential interference contrast) on a Zeiss Axiovert 135 microscope (Neumann et al., 1998). Illumination was by arc lamp (HBO 100, Zeiss Attoarc, Thornwood, NY) through a fiber-optic coupling (Technical Video Ltd., Woods Hole, MA). A water immersion objective (Zeiss Achroplan 63 X/0.90 W) was used as the condenser to allow clearance for micromanipulation and to maximize numerical aperture. Light was collected using a Zeiss 100X/1.30 oil Plan NEOFLUAR. The DIC image was then projected onto to a tube camera (Dage MTI VE1000, Michigan City, IN), or a brightfield image was directed to a linear photodiode array (K series, 1024 element wide aperture array, Reticon, Sunnyvale, CA).

Filament attachment and force measurements

Force measurements were obtained using nanofabricated cantilevers (Fig. 1) designed and constructed in collaboration with the Cornell Nanofabrication Facility (Fauver et al., 1998). Mass produced and disposable, these cantilevers can be manufactured to high precision with a range of stiffnesses (620–0.050 pN/nm thus far), and are suitable for force measurements from several piconewtons to micronewtons. Measurements on a small number of levers are sufficient to characterize the stiffness of the batch to a high degree of accuracy, ±7% to 16% (Fauver et al., 1998).

Submitted May 29, 2001, and accepted for publication February 25, 2002.

Address reprint requests to Dwayne Dunaway, Department of Bioengineering, University of Washington, Seattle, WA 98195. Tel.: 206-685-1880; Fax: 206-685-3300; E-mail: ghp@u.washington.edu.

© 2002 by the Biophysical Society

0006-3495/02/06/3128/06 $2.00

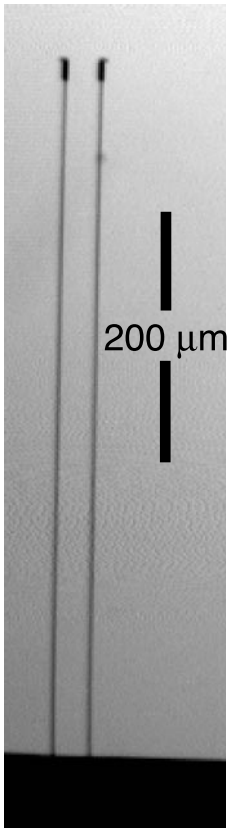

FIGURE 1 Nanofabricated cantilevers. Low strain silicon-nitride, 568-μm long, 1-μm wide, 863-nm thick.

Levers are attached to micromanipulators and imaged by optical microscopy. The nanolevers' operating principle is similar to that of glass needle transducers; force is proportional to displacement, and displacement is detected optically (Fig. 2). The base of the flexible lever pair is moved away from the stiff beam, and the filament is thereby loaded. The filament extends, and the flexible lever deflects in proportion to the load. A bright-field image of the lever tips is projected onto a linear photodiode array, providing a signal that contains lever positions (Fauver et al., 1998; Neumann et al., 1998). The signal can be analyzed to yield force ($\pm$1 pN) and filament length ($\pm$5 nm). Lever stiffness is 0.179 pN/nm in these experiments. The filament-length calculation is affected by the angle of the lever because the region of the lever projected onto the array is displaced from the filament. We have corrected for this error by subtracting (distance between filament and measurement region)*sin (lever tip angle) from the filament length.

Filament attachment is critical for this experiment and is conducted following a simple process. A filament solution is placed in the chamber; individual filaments spontaneously attach to the silicon nitride cantilevers. When attachment occurs in a desirable position and orientation, the deflectable cantilever is brought into contact with the opposite end of the filament, suspending the sample between two levers (Fig. 3).

From the DIC image it is not possible to conclusively discern between the presence of a single filament or several side by side. However, our electron micrographs imply that filaments are rarely stuck together side by side. When they attach to one another filaments usually cross at angles, sometimes forming networks. Crossed filaments and filament networks are readily detectable in DIC.

The measurement apparatus is particularly well suited for force measurements on structurally rigid filaments (i.e., high persistence length),

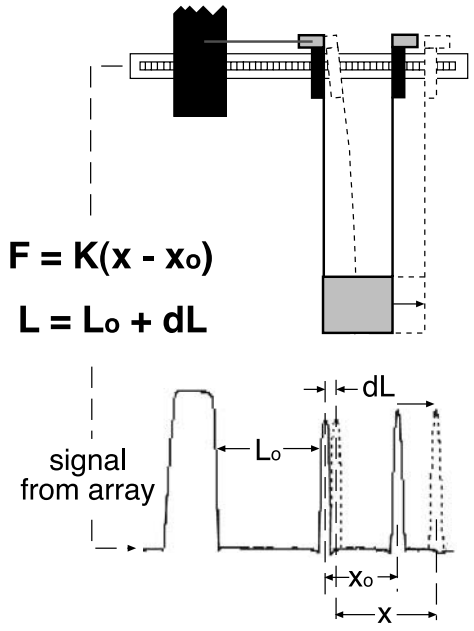

FIGURE 2 Force and length measurement scheme. F is force; L is filament length; K is lever stiffness; x is spacing between lever tips. Lever deflection (typically less than 1% of lever length) is exaggerated in this diagram.

which are unable to bend at the point of attachment. Both atomic force microscopy and optical traps require a 90° bend in the filament at the site of attachment. When small strains on the order of 2% are under consideration, any peeling or induced change in bend curvature could contribute substantially to measured force-elongation behavior. By contrast, nanofabricated cantilevers provide a large attachment surface in the same plane as the filament (Fig. 3). The filament does not bend, and the force of attachment is distributed.

RESULTS AND DISCUSSION

Synthetic thick filaments were used in this study because they can be made an order of magnitude longer than native filaments. The long length facilitates attachment and amplifies molecular length changes. The filaments used in this study were made following the protocol developed by Pinset-Harstrom and Truffy (1979). The authors used electron

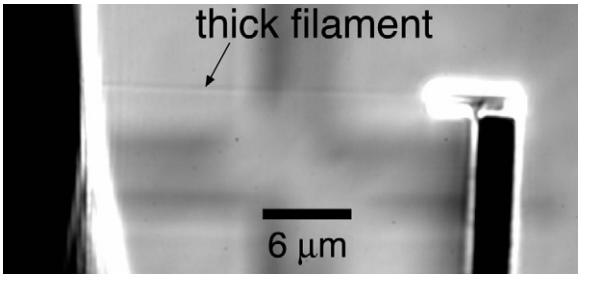

FIGURE 3 DIC image of thick filament suspended between two cantilevers. Dark regions of the cantilevers indicate where gold coating was added to provide maximal optical contrast.

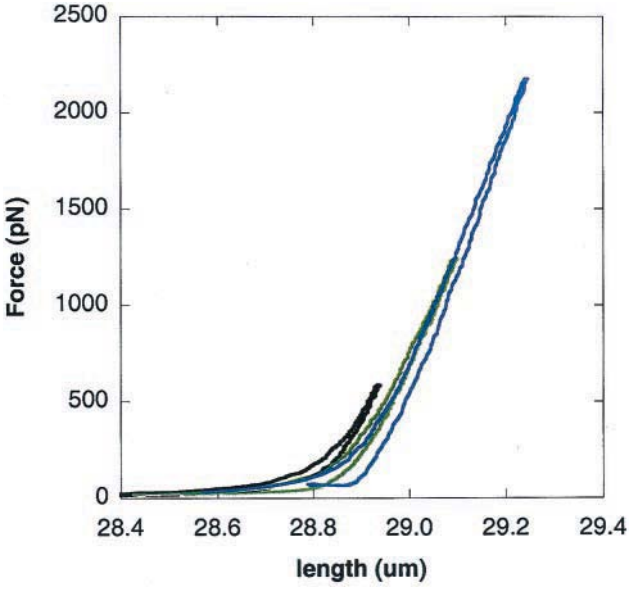

FIGURE 4 Representative force-elongation curves from the same filament with different amplitudes.

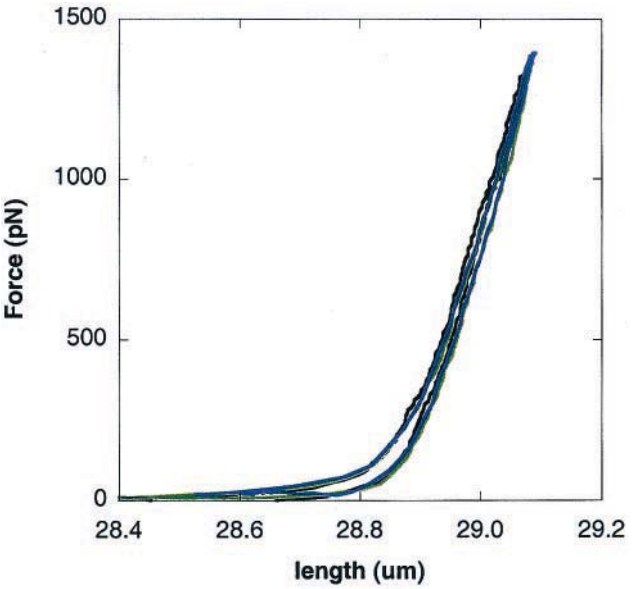

FIGURE 5 Three stretch-release cycles of equal amplitude carried out at different stretch rates. Stretch ramps extending the filament from slack to maximal extension were imposed over 0.75, 1.5, and 3.0 s, respectively.

microscopy (Pinset-Harstrom and Truffy, 1979) and optical diffraction (Morel et al., 1979) to fully characterize the filaments. Although they lack accessory proteins, the synthetic filaments used in this study are morphologically similar to native filaments, exhibiting physiological diameters (14.1 ± 1.4 nm, $n = 27$, from micrographs, data not shown), polarity reversal in the center, a 14.3-nm cross-bridge spacing, and a 43-nm helical repeat (Morel et al., 1979; Pinset-Harstrom and Truffy, 1979).

Force-elongation curves show distinct responses to varying levels of tension (Fig. 4). At low force (up to ~100 pN), filaments are highly elastic and exhibit a nonlinear relationship between stress and strain. At higher loads (in excess of ~100 pN) stiffness becomes nearly constant. These data indicate that during the initial low force stage of muscle activation, the thick filament is relatively compliant.

This portion of the curve could potentially be affected by the transition from buckled to extended state. For fixed-boundary conditions the buckling force is $4\pi^2EI/L^2$ in which $I = \pi r^4/4$ (Gere and Timoshenko, 1984). The slope from the stiffest portion of Fig. 6 was 155 nN (see Fig. 6); this is equivalent to elastic modulus times area. Assuming E to be 155 nN/πr^2, a radius (r) of 7 nm (from micrographs), and a filament length (L) of 9 to 30 μm (suspended lengths from this study), then the buckling force is 0.1 to 2 pN. These forces are small and should have little affect on measured force.

Ultimately, the physiological load on a thick filament in a fully activated muscle reaches ~440 pN in the bare zone (calculated assuming a 450 Å spacing between thick filaments in the hexagonal lattice, and active tension of 0.25 N/mm^2). This value agrees with the 440 pN calculated in another study (Suzuki and Sugi, 1983). With stretch in active muscle this value could double. Our results show elongations of 1.5 ± 0.5% (mean ± 1 SD, $n = 5$) under loads of 440 pN. Interestingly, full activation and stretch are predicted to produce tensions falling on the steeper, nearly linear portion of the force-elongation curve, yielding stiffness far higher than experienced during initial activation.

With increased stretch amplitude stiffness remains essentially constant. At higher forces (typically > 2500 pN) the filament pulls off one of the levers or breaks in the center. The silicon nitride surface of the levers seems to provide a strong attachment surface. In the past, levers have been coated with nitrocellulose to improve adhesion, but with synthetic filaments this results in a weaker attachment.

With release, the shape of the force-length curve follows the stretch curve, although there is some hysteresis. Measurements on individual thick filaments were highly repeatable; multiple stretches on the same filament yielded curves, which essentially superimposed. Among different filaments, there was some variation in the slope of the linear region.

The amount of hysteresis (determined by measuring the difference between the area under the stretch and release curves) was variable among filaments (1%–20%). Irrespective of interfilament results, measurements on individual thick filaments produced repeatable force-elongation curves with consistent hysteresis values that were independent of stretch rates (Fig. 5). However, we cannot exclude the possibility that faster stretch rates may influence the shape of the curve.

The stretch rates were varied by changing the rate of the ramp imposed by the piezo-electric element on the base of

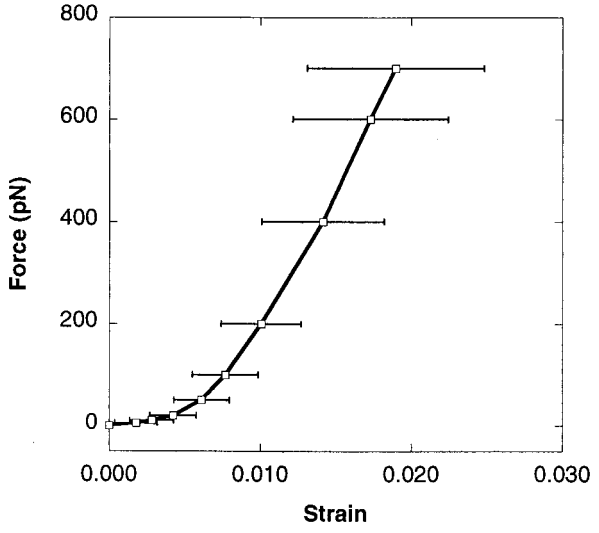

FIGURE 6 Average force-strain data. Curve generated by averaging the strains in different filaments ($n = 5$, mean $\pm$ 1 SD) at selected force levels.

the force transducer (Fig. 2). The stretch rates during a single stretch were not constant because elongation of the filament and deflection of the lever were nonlinear and linked, even though the ramp imposed by the piezo-electric was essentially linear. Deflection of the lever was approximately 10 times greater than extension of the filament. After the load increased to several hundred piconewtons the stretch rate was essentially constant. In this region of the curve in Fig. 5 stretch rates were approximately 66, 133, and 266 nm/s.

Average force-elongation curve

An average curve was constructed for comparison with x-ray diffraction data (Fig. 6). To compare the data from different filaments it was necessary to convert data to strain because the filaments measured in this study ranged in length from 9 to 28 μm. A zero-strain position was determined from the shape of the curve. This has been done in other studies by applying the wormlike chain model to extract the contour length (Kellermayer et al., 1997; Baumann et al., 1997). With thick filament data this resulted in unrealistically short persistence lengths (using Eq. 2 in Baumann et al., 1997). To determine the zero-strain position, an alternative method was developed. During experiments, filaments start off buckled and become extended during the early part of the stretch; thus, the initial part of the experiment does not correspond to zero strain. The contour length of the filaments could not be determined to high accuracy from video ($\pm$200 nm). It was assumed that the zero strain length or contour length was passed when the slope of the force-strain curve began to change. A slope of 50 pN/0.025 strain was used because it was close to the smallest detectable change in slope and because it drew data from the different filaments together.

The initial increase in force at the beginning of a stretch curve provides an indication of the extension of the filament and the zero-strain position. Data were plotted together as force versus strain and averaged at selected force levels to generate an average stretch curve. An average release curve was not generated because the initial condition, the maximal load at beginning of the release, was different in each experiment. The difference in force at maximal strain influences the shape of the release curve.

Comparison with x-ray diffraction data

Myosin heads project off the thick filament at regular intervals of 14.3 nm. As the load on muscle changes, strain in the thick filament is predicted to alter the myosin-head spacing, which should be evident in x-ray diffraction patterns. With muscle activation, x-ray diffraction patterns show a 1.0% to 1.5% shift in the reflection associated with the myosin-head spacing (Huxley and Brown, 1967; Haselgrove, 1975; Huxley et al., 1994) (i.e., there is an apparent elongation consistent with our direct observation). However, myosin reflections are also thought to be influenced by changes in position or state of the cross-bridges (Huxley et al., 1994). To determine how much of the shift in the myosin reflections might be due to filament elasticity, we have compared published x-ray diffraction data from whole muscle with our mechanical experiments on single filaments.

In mechanical experiments on isolated filaments, the load along the filament is constant; however, the in situ loading of the thick filament is more complicated. The load is transferred through the cross-bridges, which are evenly distributed along the thick filament. The load is essentially zero at the tips of the thick filament and increases to a maximum near the center. The strain would likewise vary from zero at the tips to a maximum in the center. The cross-bridges are presumed to cycle on and off dynamically, making it impossible to determine the exact distribution of the load. For the purpose of comparison in this study we make a rough approximation that the loading is linear along the thick filament and use an axially averaged force for comparison with the x-ray diffraction data (assuming 440 pN in the bare zone at maximal activation, bare zone length of 160 nm, and thick filament lengths of 1600 nm, then axially averaged force would be 240 pN).

The x-ray data (Fig. 7) are from two studies: one with real-time myosin spacing measurement in two experiments (Yagi et al., 1995) and another with average myosin spacing measurements only at specific times in many experiments (Huxley et al., 1994). The real-time x-ray diffraction data were reanalyzed to generate a plot of force versus strain. Filament data are from Fig. 6. Real-time x-ray diffraction data were from an experiment involving activation, then

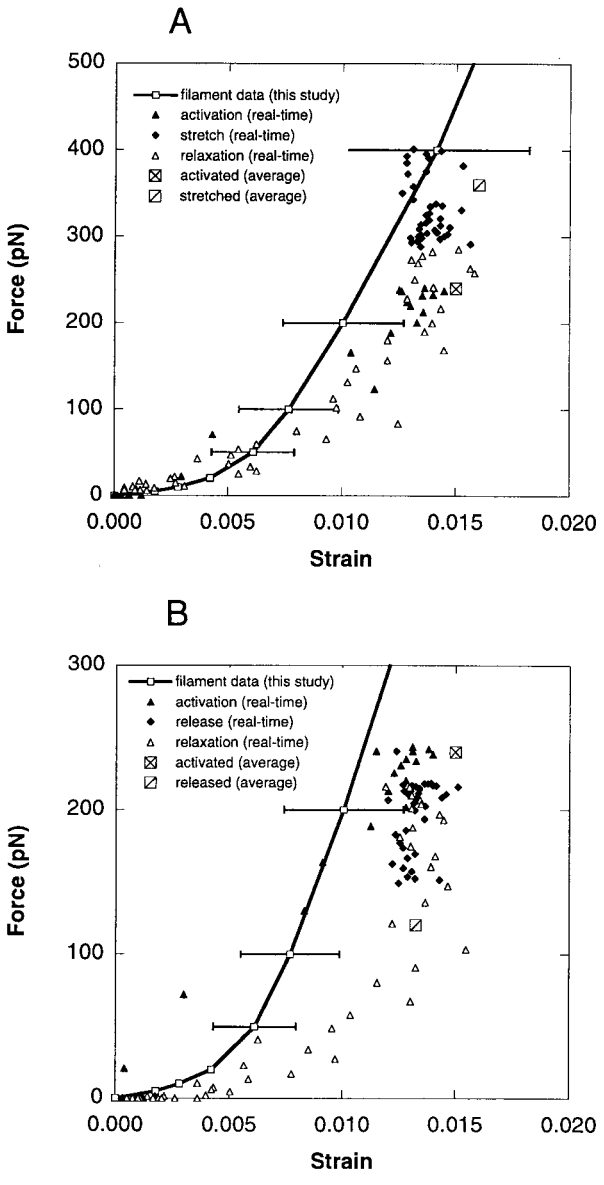

FIGURE 7 Average filament data and x-ray diffraction data. (*A*) Comparison with x-ray diffraction stretch experiments. (*B*) Comparison with x-ray diffraction release experiments.

stretch or release, and then relaxation (stimulation ceased; Yagi et al., 1995). Real-time data points were replotted as force versus strain from plots of tension versus time and third meridonal reflection spacing versus time (after Yagi et al., 1995, data from Figs. 4 *g* and 1 *a* for stretch, or Figs. 3 *g* and 1 *b* for release). Zero-strain position was taken as 14.34 nm, the average spacing at zero tension. "Average" x-ray data are from multiple experiments in which myosin spacing was measured after activation and then stretch or release (Huxley et al., 1994). All x-ray diffraction data were scaled assuming 240 pN/thick filament at full activation.

At maximal activation, the elongation is similar in x-ray diffraction data, 1.3% to 1.5% (Yagi et al., 1995; Huxley et al., 1994), and average filament data, 1.1% ± 0.3%, $n = 5$ (assuming 240 pN axially averaged). In both real-time experiments, hysteresis appears to be present in activation-relaxation paths, which agrees with force-strain curves from single filaments, often showing hysteresis (Figs. 4 and 5).

Similarity of magnitude and shape of the force elongation curve in x-ray diffraction and filament data implies that changes in the myosin reflection spacing may be due to elongation of the thick filament backbone. It has been noted that spacing changes seen during activation are far greater than changes with stretch (1.5% vs. 0.1% for a 50% increase in load; Huxley et al., 1994). This difference has been interpreted as inconsistent with a mechanism based on filament elasticity (Huxley et al., 1994; Yagi et al., 1995). Also, Huxley states that the initial increase in the reflection spacing occurs before significant force development (Huxley et al., 1994). This can be seen in the real-time data (Fig. 7); the change in myosin head spacing is rapid at the onset of contraction with a half time of 50 ms, whereas during relaxation the decrease is much slower (Yagi et al., 1995). The nonlinear shape of the filament force-elongation curve fits these observations. Because stiffness increases substantially with load, most of the spacing change is expected at low forces. The initial increase in myosin head spacing is rapid because of the initial low stiffness of the filament and the fast rise time of force upon activation. Similarly with relaxation the return of the myosin head spacing to a resting value is slow because filament is more compliant at low forces and decrease in tension to a zero value is slow compared with the increase with activation (see Fig. 1, *a* and *b* of Yagi et al., 1995).

A previous study using rigor-stretched muscle fibers reported localized elongation in the bare zone (Suzuki and Sugi, 1983). In our data we could not detect whether elongation was uniform or nonuniform. X-ray diffraction cannot detect localized length changes such as those in the bare zone because it is sensitive to average myosin head spacing. The close agreement between average filament and x-ray diffraction data implies that strain is distributed along single filaments.

Implications of in situ variable strain

The strain varies from zero at the tips to a maximum in the center, and would have a nonlinear distribution similar to the force-elongation curves shown in Figs. 4 to 6. Variable strain along the thick filament will affect the actin-myosin binding-site alignment, which in turn affects the numbers of cross-bridges able to bind as well as the theorized cycling rate (Daniel et al., 1998). In other words, strain of even 1% to 2% at the molecular level will critically impact the entire process of force development.

CONCLUSION

In sum, using a new technique, we have conducted the first force-elongation measurements on single vertebrate thick filaments. Thick filaments elongate ~1.1% under physiological forces. The magnitude and shape of the force-elongation curves are consistent with x-ray diffraction data, which implies that changes seen in the myosin reflections (Huxley et al., 1994) may represent length changes in the thick filament backbone. This result will impact interpretation of sarcomere mechanics and force generation at the molecular level.

The authors thank Bryant Chase for his donation of the myosin used in this study, as well as Jeff Magula and John Myers for their technical contributions to the experimental apparatus.

REFERENCES

Baumann, C. G., S. B. Smith, V. A. Bloomfield, and C. Bustamante. 1997. Ionic effects on the elasticity of single DNA molecules. *Proc. Natl. Acad. Sci. U. S. A.* 94:6185–6190.

Daniel, T. L., A. C. Trimble, and P. B. Chase. 1998. Compliant realignment of binding sites in muscle: transient behavior and mechanical tuning. *Biophys. J.* 74:1611–1621.

Fauver, M. E., D. L. Dunaway, D. H. Lilienfeld, H. G. Craighead, and G. Pollack. 1998. Microfabricated cantilevers for measurement of subcellular and molecular forces. *IEEE Trans. Biomed. Eng.* 45:891–898.

Ford, L. E., A. F. Huxley, and R. M. Simmons. 1977. Tension responses to sudden length change in stimulated frog muscle fibers near slack length. *J. Physiol. (Lond).* 269:441–515.

Gere, J. M., and S. P. Timoshenko. 1984. Mechanics of Materials. PWS Publishers, Boston, MA.

Gordon, A. M., M. A. LaMadrid, Y. Chen, Z. Luo, and P. B. Chase. 1997. Calcium regulation of skeletal muscle thin filament motility in vitro. *Biophys. J.* 72:1295–1307.

Higuchi, H., T. Yanagida, and Y. E. Goldman. 1995. Compliance of thin filaments in skinned fibers of rabbit skeletal muscle. *Biophys. J.* 69: 1000–1010.

Haselgrove, J. C. 1975. X-ray evidence for conformational changes in the myosin filaments of vertebrate striated muscle. *J. Mol. Biol.* 92:113–143.

Huxley, H. E., and W. Brown. 1967. The low-angle x-ray diagram of vertebrate striated muscle and its behavior during contraction and rigor. *J. Mol. Biol.* 30:383–434.

Huxley, H. E., A. Stewart, H. Sosa, and T. Irving. 1994. X-ray diffraction measurements of the extensibility of actin and myosin filaments in contracting muscle. *Biophys. J.* 67:2411–2421.

Kellermayer, M. S., S. B. Smith, H. L. Granzier, and C. Bustamante. 1997. Folding-unfolding transitions in single titin molecules characterized with laser tweezers [published erratum appears in *Science.* 1997. 277:1117]. *Science.* 276:1112–1116.

Kojima, H., A. Ishijama, and T. Yanagida. 1994. Direct measurement of stiffness of single actin filaments with and without tropomyosin using in-vitro nano-manipulation. *Proc. Natl. Acad. Sci. U. S. A.* 91: 12962–12966.

Kubota, K., B. Chu, S. F. Fan, M. M. Dewey, P. Brink, and D. E. Colflesh. 1983. Quasi-elastic light scattering of suspensions of Limulus thick myofilaments in relaxed (long) activated and rerelaxed (short) states. *J. Mol. Biol.* 166:329–340.

Margossian, S. S., and S. Lowey. 1982. Preparation of myosin and its subfragments from rabbit skeletal muscle. *Methods Enzymol.* 85:55–71.

Morel, J. E., I. Pinset-Harstrom, and A. M. Bardin. 1979. Internal structure of myosin synthetic filaments. *Biol. Cell.* 34:9–16.

Neumann, T., M. Fauver, and G. H. Pollack. 1998. Elastic properties of isolated thick filaments measured by naofabricated cantilevers. *Biophys. J.* 75:938–947.

Pinset-Harstrom, I., and J. Truffy. 1979. Effect of adenosine triphosphate, inorganic phosphate and divalent cations on the size and structure of synthetic myosin filaments. *J. Mol. Biol.* 134:173–188.

Rief, M., M. Gautel, F. Oesterhelt, J. M. Fernandez, and H. E. Gaub. 1997. Reversible unfolding of individual titin immunoglobulin domains by AFM. *Science.* 276:1109–1112.

Suzuki, S., and H. Sugi. 1983. Extensibility of the myofilaments in vertebrate skeletal muscle as revealed by stretching rigor muscle fibers. *J. Gen. Physiol.* 81:531–546.

Tskhovrebova, L., J. Trinick, J. A. Sleep, and R. M. Simmons. 1997. Elasticity and unfolding of single molecules of the giant muscle protein titin. *Nature.* 387:308–312.

Yagi, N., Y. Amemiya, and K. Wakabayshi. 1995. A real-time observation of X-ray diffraction from frog skeletal muscle during and after slow length changes. *Jap. J. Physiol.* 45:583–606.